ARTICLE

# $CuO/La_{0.5}Sr_{0.5}CoO_3$: precursor of efficient NO reduction catalyst under three-way catalysis studied by operando high energy X-ray diffraction

Received 00th January 20xx,
Accepted 00th January 20xx

DOI: 10.1039/x0xx00000x

Ivo Alxneit,[a] Alberto Garbujo,[b] Giovanni Carollo,[b] Davide Ferri,[a,*] Antonella Glisenti[b,*]

Substitution of critical raw materials such as platinum group metals in automotive catalysts is challenging. In this work we realized a nanocomposite in which CuO nanoparticles are highly dispersed on a $La_{0.5}Sr_{0.5}CoO_3$ perovskite-type oxide (LSCO). The behaviour and reactivity under three way catalyst conditions was monitored by operando time-resolved high-energy X-ray diffraction under oscillating rich/lean feed. The reducing environment converted CuO into Cu(0) in a two step process: Cu(II) to Cu(I) and to Cu(0), while the perovskite evolved to a oxygen deficient brownmillerite phase. These structural transformations are shown to be crucial for catalytic activity. The in-situ generated Cu(0)/Cu(I)/LSCO nanocomposite is active for NO reduction above 300°C, reaching 90% NO conversion at 450°C. The effect of feed composition on the diffraction patterns was studied by Rietveld refinement in order to rationalize the experimental observations under TWC conditions.

## Introduction

Three-way catalysts (TWCs) are exploited to control the emissions of gasoline vehicles.[1] Their engines are operated efficiently at stoichiometry, i.e. close to an air-to-fuel ratio equal to 14.6, commonly referred to as $\lambda = 1$.[2] Engines burning gasoline or similar fuels such as natural gas, have become even more attractive for future transportation policies due to concerns with Diesel exhaust after treatment technologies that have drawn significant negative attention from the public opinion. The expected growth of passenger vehicles equipped with stoichiometric engines, especially in heavily populated countries,[3] calls for a renewed effort in the development of catalytic exhaust after treatment technologies as well as combustion and control technologies.[4]

Next generation TWCs should comprise low amounts of expensive platinum group metals (PGM) while maintaining their high efficiency to cope with increasingly stringent emission regulations worldwide. Amongst other transition metals,[5, 6] copper is considered a potential candidate to replace PGM in gasoline emission control technologies. A recent quick X-ray absorption spectroscopy study by Nagai et al.[7] at the Cu and Ce K-edges demonstrated that Cu supported on $CeO_2$ possesses remarkable TWC properties under close to real operation conditions most notably with respect to the demanding NO reduction reaction. The NO reduction activity of $CuO/CeO_2$ increased significantly under oscillating feed relative to a static feed composition between 200 and 400°C that was attributed to the formation of oxygen vacancies and of reduced Cu species at the $CuO\text{-}CeO_2$ interface.

Perovskite-type oxides of formula $ABO_3$ have also been exploited with the same aim to reduce PGM utilization. These support materials exhibit promising TWC properties when associated with PGM.[8] Metals such as Pd and Rh that are used as active phases for CO and hydrocarbon oxidation as well as NO reduction, respectively, can be reversibly incorporated into and segregated out of the perovskite-type structure under the oscillating feed conditions of TWCs.[9, 10] Catalytic metals in such systems are also stable against sintering and preserve their high dispersion. They are therefore able to maintain their high activity during long-term operation. Perovskite-type oxides have been also shown to be ideal precursors of materials with unique interfacial properties upon exsolution of metals under reducing conditions.[11]

Recently, some of the authors demonstrated the potential of Cu-containing perovskite-type oxides. Cu inserted within the lattice of mixed oxides of the $La_{1-x}Sr_xCo_{1-y}Cu_yO_3$ type exsolves at the surface under reducing conditions. At this point the reactivity, particularly towards NOx, appears.[12] The formation of $Cu/LaCoO_3$ enhances the low temperature activity if care is taken to obtain high dispersion of the Cu nanoparticles.[13] The use of perovskite-type oxide supports allows to obtain diversified reactivity: in $Cu/LaNiO_3$ systems, for example, NO reduction is favoured by the $H_2$ formed by reforming of hydrocarbons catalysed by nickelates.[14] $CuO/La_{0.5}Sr_{0.5}CoO_3$ was shown to be the most active catalyst of the $La_{1-x}Sr_xCoO_3$ series.[15] $La_{0.5}Sr_{0.5}CoO_3$ is expected to exhibit higher oxygen mobility and exchange capability,[15, 16] properties that affect the Cu-perovskite interface and thus the reactivity.[17]

[a] Paul Scherrer Institut, CH-5232, Villigen PSI, Switzerland.
[b] Università degli Studi di Padova, Dipartimento di Scienze Chimiche, I-35131, Padova, Italy.

† PCCP themed issue: Synchrotron Radiation Techniques in Catalytic Science.

View Article Online
DOI: 10.1039/D0CP01064B





In this work, we analyse the catalytic performance of a $CuO/La_{0.5}Sr_{0.5}CoO_3$ catalyst under alternating rich/lean redox conditions while acquiring operando time-resolved high-energy X-ray diffraction (XRD) patterns to follow structural changes associated with its catalytic activity determined simultaneously by mass spectrometry. XRD is an ideal method to follow structural changes of this type of materials under these conditions because of the rich chemistry of perovskite-type oxides and of the sufficiently high loading of CuO. Information on all phases composing the material can be followed with high time resolution of 2 Hz.[18] With the aid of XRD, we provide new insights into the chemistry of $CuO/La_{0.5}Sr_{0.5}CoO_3$ used as potential TWC that may aid development of PGM-free catalysts. In particular, we demonstrate that: (i) $CuO/La_{0.5}Sr_{0.5}CoO_3$ is able to reduce NO only when operated under oscillating feed conditions and in the presence of propene as representative hydrocarbon for gasoline operation. (ii) The perovskite host strongly reacts to the oscillating feed at temperatures just below the light-off of NO reduction. (iii) At temperatures above about 250°C the perovskite reversibly transforms to a brownmillerite phase. (iv) Cu/brownmillerite is the active catalyst for efficient NO reduction under these conditions.

## Experimental

### Catalyst preparation and characterization

$La_{0.5}Sr_{0.5}CoO_3$ was prepared by the amorphous citrate method starting from $La_2O_3$ (Sigma-Aldrich, 99.9%), $Sr(NO_3)_2$ (Sigma-Aldrich, 99%) and CoO (Acros, 99%). After complete dissolution of the precursors with nitric acid (68 vol% in water), the final solution was heated at 80 °C to promote solvent evaporation and obtain a wet-gel, which was then treated in air at 400 °C for 2 h to decompose the organic framework. The ash-like material was calcined in air at 900 °C (heating rate 6 °C/min) for 6 h to obtain the desired perovskite phase. The calcined $La_{0.5}Sr_{0.5}CoO_3$ was impregnated with $Cu(NO_3)_2$ (Sigma-Aldrich) by the ammonia deposition preparation method[17] in order to achieve 20 wt% CuO loading. Finally, the material was calcined at 550°C for 8 h.

The specific surface area was measured by $N_2$ physisorption at the temperature of liquid $N_2$ using an Autochem II 2920 instrument (Micromeritics) and the Brunauer-Emmet-Teller (BET) equation. Prior to $N_2$-sorption, the sample was degassed at 200 °C for 16 h. The phase composition was determined by X-ray diffraction using a Bruker Advance diffractometer (Cu Kα source). Transmission electron micrographs were obtained using a probe corrected JEOL JEM-ARM200F (NeoARM) microscope equipped with a cold field emission gun operated at 200 keV and a Gatan OneView camera.

### High-energy X-ray diffraction

Operando time-resolved X-ray diffraction patterns were acquired at beamline ID15A of the ESRF (Grenoble, France, beam size 100×100 µm) using a Pilatus X detector (1679x1475 pixels, Dectris) at a time resolution of 0.5 s and at an incident energy of 74.89 keV. The sample (24.5 mg; sieve fraction, 100-150 µm) was firmly mounted between two quartz wool plugs in a custom-made cell[19] equipped with two graphite windows and installed at a distance of 446 mm from the detector. The cell was connected to a gas manifold allowing for fast switching of the feed to simulate TWC operation and was interfaced by heated stainless steel capillary to a mass spectrometer (MS, Pfeiffer Omnistar GSD 320) for on-line gas analysis. The following m/z values were recorded: 2 ($H_2$), 4 (He), 18 (water), 28 (CO, $N_2$), 30 (NO), 32 ($O_2$), 44 ($CO_2$, $N_2O$) and 46 ($C_3H_6$). Feed conditions were controlled by two solenoid on/off valves (Series 9, Parker; opening time ≤5 ms) placed in front of the cell and slaved to the beamline control software to synchronize data acquisition and gas switches. Under rich conditions the feed composition was 0.7 vol% CO, 0.15 vol% NO, 0.16 vol% $C_3H_6$ balanced with He. When 0.7 vol% $O_2$ was added, the feed composition was only slightly lean. Experiments under constant feed were performed with 0.7 vol% CO, 0.15 vol% NO, 0.16 vol% $C_3H_6$, 1 vol% $O_2$, balanced with He. Rich or lean feed conditions were maintained for 20 s each. The long pulse time and the predominantly rich reaction conditions relative to realistic operation are suitable from an experimental viewpoint to study the catalytic and structural response. The large difference in oxygen concentration, much larger than expected for operation in real, was selected to enhance the chemical response and possible structural changes.[7] Sample temperature was monitored continuously using a K-type thermocouple inserted longitudinally in the inlet of the catalyst bed (<1 mm within the bed) and interfaced to the MS. Before performing catalytic experiments, the sample was treated in 5 vol% $O_2$/He (50 ml/min) at 400°C for 30 min. Data was collected during temperature ramps between 100 and 450°C (10°C/min) in either alternating or continuous feed conditions. Additional experiments were carried out at 400°C with and without propene in the feed.

### Rietveld analysis

Rietveld analysis of the time resolved XRD data was performed by GSAS-II.[20] Typically, data analysis was restricted to the range $3.0<2\theta<17.5$ ($3.16>Q>0.544$ Å$^{-1}$) and the background was modelled with a Chebychev polynomial of order 7. As no error estimate for the counts was provided, σ= counts$^{½}$ was used, i.e. assuming Poisson noise. Exclusively $La_{0.5}Sr_{0.5}CoO_3$, $La_{0.5}Sr_{0.5}CoO_{2.5}$ (brownmillerite, a reduced perovskite with ordered oxygen vacancies), CuO, $Cu_2O$, and Cu were used to model the pattern. Only unit cell parameters and weight fractions could be modelled for all phases due to the relatively low resolution of the data. The half-width of the most intense peak of $La_{0.5}Sr_{0.5}CoO_3$ at $2\theta= 3.475$ ($Q= 2.73$ Å$^{-1}$) is only about 4-5 data points. Thus, parameters determined by the exact line shape were difficult to model. Particles sizes could be obtained for most of the phases as long as the weight fraction was sufficiently high. Series of several thousand diffraction patterns were analysed. For some isolated patterns of the series a different local minimum was found which lead to spikes in the resulting curves. These spikes were removed by treating the raw curves with a moving median filter with a window of 11 data points corresponding to a time window of 5.5 s, much lower than the length of the uniform feed segments.

DOI: 10.1039/D0CP01041B

## Results and Discussion

The catalytic material (4.6 $m^2/g$) initially comprised of CuO nano-particles of 5-10 nm diameter deposited on dense particles of $La_{0.5}Sr_{0.5}CoO_3$ as shown in Figure 1a.

In Figure 2 we report (a) the catalytic activity and (b) the 2D map of the time-resolved high-energy powder diffraction patterns of $CuO/La_{0.5}Sr_{0.5}CoO_3$ exposed to alternating rich/lean gas conditions while temperature was increased from 100°C to 450°C and then decreased to 100°C again. Initially, at temperatures below 200°C, the system did not respond to the alternating feed conditions (Figure 2(a)). CO, $C_3H_6$, and NO concentrations remained virtually constant and $CO_2$ was not formed. The small spikes are pressure transients caused by switching the feed. From about 150°C CO started to be oxidized to $CO_2$. Once temperature increased further to 300°C, propene started to be oxidized, CO concentration decreased simultaneously to $CO_2$ formation. The concentrations of these gases clearly followed the oscillating feed conditions. In the same temperature interval the NO concentration started to oscillate strongly, while hardly any net reduction could be detected (mean NO conversion below 5%). Only once the peak temperature of 450°C was reached, NO was reduced substantially reaching a mean conversion close to 90%. Considering a mean NO concentration during the lean segments, 50% conversion was reached at 427°C ($T_{50}$). During cooling, NO reduction extended down to ca. 300°C ($T_{50}$= 343°C) revealing the presence of a conversion hysteresis with $\Delta T_{50}$= 84°C between heating and cooling segments. In the absence of more suitable gas phase analytics, we cannot conclude about the evolution of both $N_2O$ and $NH_3$ as possible intermediates because their m/z values are masked by $CO_2$ and water, both major products of the reactions.

An overview of the structural changes occurring during the experiment is reported in Figure 2(b). The operando high-energy XRD data demonstrate that the initially present CuO (2.483 and 2.699 $Å^{-1}$) started to reduce to $Cu_2O$ at around t= 1500 s (ca. 300°C; 2.546 $Å^{-1}$), while $Cu_2O$ was further reduced to metallic copper (2.978 $Å^{-1}$) above ca. 400°C. In the interval 1500 < t < 4000 s structural changes of the perovskite were also observed. The main diffraction peaks at 2.3 and 3.25 $Å^{-1}$ broadened, lost intensity and shifted to lower Q values. Selected XRD patterns corresponding to t= 0 s (bottom most pattern), intermediate times (numbered patterns), and at the end of the experiment (top most pattern) are reported in Figure 3(a). CuO initially present in the pattern 1 (room temperature) disappeared as $Cu_2O$ was formed above 340°C (pattern 2), which further reduced to metallic Cu at ca. 440°C (pattern 3). In the cooling segment, $Cu^0$ persisted until t= ca. 3700 s (ca. 375°C) and was oxidized to $Cu_2O$, but not completely. Reoxidation to the initial CuO was not observed. This behaviour is consistent with thermodynamic equilibrium calculations[21] revealing CuO to be the only copper phase present in equilibrium with air at room temperature. Copper in the presence of the rich gas atmosphere is present as Cu only, while in the presence of the rich/lean atmosphere $Cu_2O$, Cu, and CuO are found (the exact amounts depend on the molar ratio of copper versus gas and on λ). Structural changes of the perovskite can be followed by observing the temporal evolution of the intense (110) reflection at ca. 2.3 $Å^{-1}$ (ca. 32.5° for Cu Kα) reported in Figure 3(b). Initially a continuous shift of the diffraction peak to lower Q-values caused by lattice expansion due to thermal expansion and, most probably, also due to partial reduction, i.e. the formation of oxygen vacancies, can be observed. After ca. 1500 s (ca. 350°C) the perovskite peak largely disappeared while a new peak at ca. 2.25 $Å^{-1}$ appeared. This new peak is attributed to brownmillerite ($La_{0.5}Sr_{0.5}CoO_{2.5}$), a reduced perovskite with ordered oxygen vacancies.[22] Once temperature was lowered, the brownmillerite disappeared and the parent perovskite was formed again at t≈ 3700 s (ca. 330°C). As temperature continued to decrease, the peaks shifted to higher Q values indicating that the perovskite-type lattice slowly contracted. Small oscillations of the perovskite peak are visible at t< 1500 s that coincide with the oscillations of the gas composition. The absence of visible structural changes within this time (< 300°C) suggests that $CuO/La_{0.5}Sr_{0.5}CoO_3$ can catalyse CO oxidation.

More detailed information on the structural changes occurring during the thermal cycle under alternating rich/lean conditions can be obtained from the Rietveld analysis. The time evolution of the weight fractions of the five phases considered is reported in Figure 4. The steps observed in the mass fractions at t= 625 s are artefacts, because brownmillerite as well as $Cu_2O$ and Cu were included in the refinement only from this point onwards. Initially, the sample consists of $La_{0.5}Sr_{0.5}CoO_3$ and CuO (80/20 by weight) as expected. Already at low temperatures a small fraction (less than ca. 3%) of brownmillerite is observed. At about t= 1200 s (250°C) CuO started to reduce to $Cu_2O$ while Cu only started to form once CuO had disappeared completely. During the high temperature segment copper was mostly present in metallic form (80%) and $Cu_2O$ (20%) while ca. 70% of $La_{0.5}Sr_{0.5}CoO_3$ was converted to brownmillerite towards the end of the high temperature segment. Once temperature was decreased to the starting value (100°C) the perovskite recovered to about 90% at the end of the experiment, while copper was mostly present as $Cu_2O$ (65%) and Cu (35%). Figure 4 demonstrates that the hysteresis in NO conversion between heating and cooling segments observed in Figure 2 was mirrored by an hysteresis in Cu reduction and reoxidation.

Interestingly, the system reacted much slower during heating than while cooling. This is notable from the interconversion of $La_{0.5}Sr_{0.5}CoO_3$ and brownmillerite as well as of the different copper phases. Furthermore, the oscillations of the gas atmosphere were clearly mirrored by the $La_{0.5}Sr_{0.5}CoO_3$/brownmillerite equilibrium. However, the largest amplitudes of this oscillation were found at low temperature (850 < t < 1450 s, 200 < T < 300°C) before significant catalytic activity could be observed. Strong oscillations were again observed once cooling started at 3500 < t < 3950 s (360-300°C). The quality of the refinement, $R_{wp}(t)$, reported in the upper panel of Figure 4 is relatively constant but rather high mainly because of the presence of some minority phases that we were not able to identify. These impurities seem to be unaffected by

View Article Online
DOI: 10.1039/D0CP01064B



the chemistry that took place during the temperature cycle and can be safely neglected when interpreting the data.

Unit cell dimensions (a, c parameter) as well as the occupancy of the oxygen site and its fractional coordinate also reflect the oscillations of the gas atmosphere. The results reported in Figure 5 are limited to the interval where the strongest oscillations were observed. To make the four curves easier to compare the relative change of each parameter is reported scaled with its mean value. Interestingly, the structural changes are evident from all parameters apart from the unit cell c parameter that linearly increases because of the thermal expansion of the lattice (Figure 5b). The response of the unit cell a parameter (Figure 5a) and of the oxygen site occupancy (Figure 5c) are out of phase with each other. Thus, the expansion of the lattice is indeed partially caused by its (partial) reduction. Finally, also the fractional oxygen coordinate (Figure 5d) follows the changes of the gas atmosphere.

The structure obtained at the minimum of $a/a_{mean}$ at t= 1242.5 s is compared with that at the following maximum at t= 1268.5 s in Figure 6 corresponding to a temperature difference of ca. 3°C at around 255°C. Only one layer of the oxygen octahedra (perpendicular to the c-axis) is displayed for clarity. Arrows depict the displacement of the corresponding atoms exaggerated by a factor of 250. Clearly, all motions are restricted to the a-b plane as imposed by the symmetry of the structure (R-3ch). The oxygen octahedra rotate around their 3-fold axis parallel to c, while at the same time they are slightly displaced from each other as shown by the red arrows indicating movement of the position of Co at their centre. This illustrates that only a change in the unit cell a parameter is expected while the structure oscillates.

A markedly different behaviour is observed if the experiment is performed in a constant gas atmosphere corresponding to λ= 0.7. Figure 7(a) reports the time evolution of the diffraction patterns as the temperature is increased from 100°C to 450°C. As this experiment was performed with the sample used in the experiment reported in Figure 2, $Cu_2O$ and Cu instead of CuO were present initially. This was further confirmed by analysis of the lattice fringes of various particles in the TEM images (Figure 1b). Figure 7(a) shows that both phases are oxidized to CuO above 300°C. This can be rationalized by noting that the average λ is only about 0.35 in an experiment with alternating rich/lean conditions. From Figure 4 we know that the different copper phases react slowly to the changing feed conditions as no oscillations are observed in their molar fractions. We therefore expect the stability of the different copper phases to be defined by the average oxygen concentration (λ). Thermodynamic equilibrium calculations suggest that at λ= 0.7 and 450°C CuO is the only stable phase, while at λ= 0.35 both Cu and $Cu_2O$ are stable. Also $La_{0.5}Sr_{0.5}CoO_3$ exhibits a different behaviour in this experiment because conversion to brownmillerite was not observed. On the contrary, the crystallinity of the perovskite-type oxide seems to increase as heating proceeds, which is evidenced by the narrowing of its diffraction peaks. At the same time, catalytic activity ceases almost completely as evidenced from Figure 7(c, d). Only oxidation of CO starting around 200°C and combustion of propene above about 325°C were observed. However, NO reduction was negligible and peak conversion of NO at 450°C was limited to about 10%.

To compare, the result of the experiment performed on the same sample under alternating rich/lean atmosphere is reported in Figures 7(b, e, f). Clearly, the same behaviour as reported in Figure 2 is observed again. Comparing the NO conversion in Figures 7(d, f) it seems that two temperature windows for NO conversion exist. Minor conversion is observed under both conditions around 300°C that is evidenced by a first plateau in Figure 7(d) or a shallow peak in Figure 7(f). The efficient NO conversion at 450°C, however, was observed only under alternating rich/lean atmosphere (Figure 7(e-f)). Additional control experiments contributed to demonstrate that (i) the combination of perovskite-type oxide and CuO is required because no CuO reduction and poor NO reduction activity were observed under identical conditions on 6 wt% $CuO/La_2O_3$ and (ii) NO reduction activity was not observed in the absence of propene on $La_{0.5}Sr_{0.5}CoO_3$. Thus, CO alone does not serve as the reducing agent in this catalytic system.

To shed additional light onto the reaction mechanism isothermal experiments at 400°C were performed with and without propene in the feed (Figure 8). The time-resolved XRD pattern for the case with propene in the feed (Figure 8a) shows that the initially present CuO was converted to $Cu_2O$ within 200 s and after about 600 s Cu dominated. Similarly, the perovskite oxide was completely converted to brownmillerite after about 500 s. In absence of propene (Figure 8b) the phases initially present in the sample were stable and only traces of $Cu_2O$ were observed. Gas analysis shows (Figure 8c) that steady state conditions were reached about 500 s after switching of the feed had been initiated as suggested by the rising of the oscillating propene signal. The initially small amplitudes of the oscillation of the different gas concentrations increased. The NO concentration started to decrease at around 500 s. From the same time on, $H_2$ could be detected and continuously increased until the end of the experiment concomitantly to the increase in NO conversion. In contrast, only small traces of $H_2$ and no NO conversion were observed when propene was not present in the feed (Figure 8d). The concentrations of all gases displayed only small oscillations around their initial value except for $O_2$, pointing to the scarce activity under these conditions.

Based on our data, we provide a tentative explanation of the overall reaction scheme that is in agreement with previous resuls on $LaNiO_3$-based materials.[14] Propene is the source of $H_2$ that drives the reduction of CuO and of the native perovskite to form the catalytically active Cu/brownmillerite system. Alternating rich/lean conditions strongly increase both reaction rates because apparent diffusion rates in the solids are strongly enhanced as all phases constantly form and are partly consumed again in each redox cycle. $H_2$ required for the reduction is formed once propene starts decomposing above 250°C according to the reaction scheme of

$$C_3H_6 + 6H_2O \rightarrow 9H_2 + 3CO_2 \quad (1)$$

i.e. steam reforming of hydrocarbons that is catalysed by mixed metal oxides such as perovskite-type oxides.[14, 23] Water

View Article Online DOI: 10.1039/D0CP01064B



required for this reaction is likely generated by propene oxidation

$$2C_3H_6 + 9O_2 \rightarrow 6CO_2 + 6H_2O \quad (2)$$

that takes place during the lean (oxygen richer) phase of the redox cycle (λ= 1 in the present case). Probably only a small fraction of propene reacts initially, but the water produced accumulates over time and increasingly promotes the steam reforming reaction. Simultaneously, the water gas shift reaction

$$CO + H_2O \rightarrow H_2 + CO_2 \quad (3)$$

consumes CO and water can act as additional source of $H_2$. $H_2$ produced by these reactions is consumed during the reduction of $La_{0.5}Sr_{0.5}CoO_3$ to brownmillerite ($La_{0.5}Sr_{0.5}CoO_{2.5}$) and the two-steps reduction of CuO to metallic copper:

$$2Cu^{II}O + H_2 \rightarrow Cu^{I}_2O + H_2O \quad (4a)$$
$$Cu^{I}_2O + H_2 \rightarrow 2Cu^0 + H_2O \quad (4b)$$

Finally, once $Cu^0$ is available, NO reduction is also observed.

$$2NO + 2H_2 \rightarrow N_2 + 2H_2O \quad (5)$$

These last three reactions, most notably the continuous NO reduction, generate water, which sustains both the steam reforming and the water gas shift reactions i.e. the two sources of hydrogen.

The operando time-resolved XRD data demonstrate that the Cu/brownmillerite system is the active catalyst. Various observations confirm this point. First, the hysteresis in NO reduction observed in the measurement of Figure 2 between heating and cooling segments is mirrored by the hysteresis in reduction of CuO to $Cu^0$ and re-oxidation only to $Cu_2O$. The brownmillerite phase is present in the same temperature range of this transformation and the perovskite is recovered upon cooling. In the subsequent heating segment (Figure 7b,e,f), the behaviour of the catalyst is identical to that observed in the cooling segment of Figure 2 rather than to the heating segment. Propene is required in the feed under pulsed conditions in order to drive the reduction of the material to the active phase. Hence, $CuO/La_{0.5}Sr_{0.5}CoO_3$ is not the active catalyst; it serves as the precursor of the active phase and does not show appreciable catalytic activity for NO reduction.

## Conclusions

In this work, we have demonstrated the potential of a perovskite supported copper catalysts for TWC applications. The activity of $CuO/La_{0.5}Sr_{0.5}CoO_3$ is correlated not only with reversible structural and chemical changes that have been followed by operando time-resolved high energy X-ray diffraction but also to the peculiar operation conditions, i.e. alternating rich and lean feed conditions. $CuO/La_{0.5}Sr_{0.5}CoO_3$ is active for CO oxidation. Both the $La_{0.5}Sr_{0.5}CoO_3$ perovskite and CuO are reduced only under alternating feed conditions to brownmillerite and metallic Cu. The resulting material is active for NO reduction above 300°C reaching 90% NO conversion at 450°C. Improvement can be foreseen with regard to the temperature at which NO reduction occurs by optimizing the perovskite composition, Cu loading and optimization of the control parameters. Therefore, suitable Cu-based perovskite-type oxide TWC might be developed for future after-treatment technologies that do not rely on PGM. The brownmillerite phase obtained during reaction is however difficult to obtain by synthesis so that we anticipate that development of the active catalyst needs to rely on a perovskite precursor. The results indicate that also the operating conditions might be optimized for this type of materials relative to benchmark TWC.

## Conflicts of interest

There are no conflicts to declare.

## Acknowledgements

The European Synchrotron Radiation Facility (ESRF) is acknowledged for beamtime allocation at beamline ID15A. The continuous support by Dr. M. Di Michiel, Dr. S. Checchia and the team of the beamline is greatly appreciated. G. Perin is thanked for support during beamtime. Prof. P. Cool (university of Antwerp) is acknowledged for support with the deposition precipitation synthesis. The Swiss National Science Foundation (SNF) is kindly acknowledged for co-funding of the electron microscope (R'Equip project 206021_177020). D.F. kindly acknowledges SNF for financial support (200021_159568). The research work carried out by authors from University of Padova was developed in the frame of the H2020 project PARTIAL PGMs project n° 686086 ('Development of novel, high performance hybrid TWC/GPF automotive after treatment systems by rational design').

## References

1. Gandhi, H. S.; Graham, G. W.; McCabe, R. W., Automotive exhaust catalysis. *J. Catal.* **2003,** 216, 433.
2. Heck, R. M.; Farrauto, R. J.; Gulati, S. T., *Catalytic Air Pollution Control*. 3rd ed.; John Wiley & Sons, Inc.: Hoboken, New Jersey, 2009.
3. Wu, Y.; Zhang, S.; Hao, J.; Liu, H.; Wu, X.; Hu, J.; M.P.Walsh; T.J.Wallington; Zhang, K. M.; Stevanovic, S., On-road vehicle emissions and their control in China: A review and outlook. *Sci. Total Env.* **2017,** 574, 332.
4. Pischinger, S., *Top. Catal.* **2016,** 59, 834.
5. Hirata, H., Recent Research Progress in Automotive Exhaust GasPurification Catalyst. *Catal. Surv. Asia* **2014,** 18, 218.
6. Beniya, A.; Ikuta, Y.; Isomura, N.; Hirata, H.; Watanabe, Y., Synergistic Promotion of NO-CO Reaction Cycle by Gold and NickelElucidated using a Well-Defined Model Bimetallic Catalyst Surface. *ACS Catal.* **2017,** 7, 1369.
7. Nagai, Y.; Dohmae, K.; Nishimura, Y. F.; Kato, H.; Hirata, H.; Takahashi, N., Operando XAFS study of catalytic NO reduction over $Cu/CeO_2$: the effect of copper–ceria interaction under periodic operation. *PCCP* **2013,** 15, 8461.

8. Royer, S.; Duprez, D.; Can, F.; Courtois, X.; Batiot-Dupeyrat, C.; Laassiri, S.; Alamdari, H., Perovskites as Substitutes of Noble Metals for Heterogeneous Catalysis: Dream or Reality. *Chem. Rev.* **2014,** 114, 10292.
9. Nishihata, Y.; Mizuki, J.; Akao, T.; Tanaka, H.; Uenishi, M.; Kimura, M.; Okamoto, T.; Hamada, N., Self-regeneration of a Pd-perovskite catalyst for automotive emissions control. *Nature* **2002,** 418, 164.
10. Tanaka, H.; Taniguchi, M.; Uenishi, M.; Kajita, N.; Tan, I.; Nishihata, Y.; Mizuki, J.; Narita, K.; Kimura, M.; Kaneko, K., Self-Regenerating Rh- and Pt-Based Perovskite Catalysts for Automotive-Emissions Control. *Angew. Chem.* **2006,** 45, 5998.
11. Neagu, D.; Papaioannou, E. I.; Ramli, W. K. W.; Miller, D. N.; Murdoch, B. J.; Menard, H.; Umar, A.; Barlow, A. J.; Cumpson, P. J.; Irvine, J. T. S.; Metcalfe, I. S., Demonstration of chemistry at a point through restructuring and catalytic activation at anchored nanoparticles. *Nat. Commun.* **2017,** 8, 1855.
12. Glisenti, A.; Pacella, M.; Guiotto, M.; Natile, M. M.; Canu, P., Largely Cu-doped $LaCo_{1-x}Cu_xO_3$ perovskites for TWC: toward new PGM-free catalysts *Appl. Catal. B* **2016,** 180, 94.
13. Pacella, M.; Garbujo, A.; Fabro, J.; Guiotto, M.; Xin, Q.; Natile, M. M.; Canu, P.; Cool, P.; Glisenti, A., PGM-free $CuO/LaCoO_3$ nanocomposites: new opportunities for TWC application. *Appl. Catal. B* **2018,** 227, 446.
14. Perin, G.; Fabro, L.; Guiotto, M.; Xin, Q.; Natile, M. M.; Cool, P.; Canu, P.; Glisenti, A., $Cu@LaNiO_3$ based nanocomposites in TWC applications *Appl. Catal. B* **2017,** 209, 214.
15. Garbujo, A.; Pacella, M.; Natile, M. M.; Guiotto, M.; Fabro, J.; Canu, P.; Glisenti, A., On A-doping strategy for tuning the TWC catalytic performance of perovskite based catalysts. *Appl. Catal. B* **2017,** 544, 94.
16. Glisenti, A.; Vittadini, A., On the Effects of Doping on the Catalytic Performance of $(La,Sr)CoO_3$. A DFT Study of CO Oxidation Catalysis. *Catalysts* **2019,** 9, 312.
17. Carollo, G.; Garbujo, A.; Xin, Q.; Fabro, J.; Cool, P.; Canu, P.; Glisenti, A., $CuO/La_{0.5}Sr_{0.5}CoO_3$ nanocomposites in TWC. *Appl. Catal. B* **2019,** 255, 117753.
18. Ferri, D.; Newton, M. A.; DiMichiel, M.; Chiarello, G. L.; Yoon, S.; Lu, Y.; Andrieux, J., Revealing the Dynamic Structure of Complex Solid Catalysts Using Modulated Excitation X-ray Diffraction. *Angew. Chem. Int. Ed.* **2014,** 53, 8890.
19. Chiarello, G. L.; Nachtegaal, M.; Marchionni, V.; Quaroni, L.; Ferri, D., Adding diffuse reflectance infrared Fourier transform spectroscopy capability to extended x-ray-absorption fine structure in a new cell to study solid catalysts in combination with a modulation approach. *Rev. Sci. Instrum.* **2014,** 85, 074102.
20. Toby, B. H.; VonDreele, R. B., GSAS-II: the genesis of a modern open-source all purpose crystallography software package. *J. Appl. Crystallogr.* **2013,** 46, 544.
21. *HSC Chemistry*, 5.1; Outokumpu Research Oy: Pori, Finland, 2002.
22. Ovenstone, J.; White, J. S.; Misture, S. T., Phase transitions and phase decomposition of $La_{1-x}Sr_xCoO_{3-\delta}$ in low oxygen partial pressures. *J. Powder Sources* **2008,** 181, 56.
23. Mawdsley, J. R.; Krause, T. R., Rare earth-first-row transition metal perovskites as catalysts for the autothermal reforming of hydrocarbon fuels to generate hydrogen. *Appl. Catal. A* **2008,** 334, 311.

DOI: 10.1039/D0CP01064B

## Figure Captions

**Figure 1.** TEM images of (a) pristine and (b) used $CuO/La_{0.5}Sr_{0.5}CoO_3$. Lattice fringes evidencing (a) CuO and (b) Cu, $Cu_2O$ and $La_{0.5}Sr_{0.5}CoO_3$ (LSCO) are indicated. The used sample derives from the experiment shown in Figure 2.

**Figure 2.** Consecutive up/down temperature ramps under alternating rich/lean feed. (a) Mass spectrometry data of m/z signals at 18 ($H_2O$), 28 (CO), 30 (NO), 32 ($O_2$), 44 ($CO_2$) and 46 ($C_3H_6$). (b) 2D representation of the corresponding operando time-resolved XRD patterns obtained at 0.5 s time resolution. Reflections indicative of the different copper species are labelled. A short interruption of the pulsing occurred mistakenly at ca. 3250 s.

**Figure 3.** (a) Representative XRD patterns obtained during the dataset of Figure 2. Copper phases are indicated in the legend. Main reflections: LSCO, $La_{0.5}Sr_{0.5}CoO_3$; br, brownmillerite. Vertical dash lines serve to guide the eye. (b) Selected area showing the behaviour of the p-b transition in the heating and cooling segments of the temperature programmed ramp. Vertical dash lines indicated time of recording of patterns shown in (a) and numbered 1-3. Left hand side is ca. 200°C, right hand side is 100°C.

**Figure 4.** Time evolution of phase composition and quality of refinement ($R_{wp}$) for the dataset of Figure 2. LSCO, $La_{0.5}Sr_{0.5}CoO_3$; br, brownmillerite.

**Figure 5.** Time evolution of relative unit cell parameters (a) $a/a_{mean}$, (b) $c/c_{mean}$, (c) oxygen site occupancy ($frac/frac_{mean}$) and (d) fractional coordinate ($x/x_{mean}$). Error bars are also shown.

**Figure 6.** Schematic representation of the rotation of the $CoO_6$ octahedra caused by partial reduction of $La_{0.5}Sr_{0.5}CoO_3$ as seen (a) perpendicular to the c-axis and (b) along the c-axis. Green and red arrows indicate displacement of oxygen and Co atoms (center of octahedra), respectively.

**Figure 7.** Operando time-resolved XRD patterns obtained on $CuO/La_{0.5}Sr_{0.5}CoO_3$ during experiments under (a) constant feed corresponding to $\lambda$= 0.7 and (b) alternating rich/lean feed (20 s). Corresponding (c, e) mass spectrometry data (m/z = 28, CO; 30, NO; 32, $O_2$; 44, $CO_2$; 46, $C_3H_6$) and (d, f) NO conversion.

**Figure 8.** Operando time-resolved XRD patterns obtained on $CuO/La_{0.5}Sr_{0.5}CoO_3$ at 400°C in alternating rich/lean feed (30 s) (a) in presence and (b) in absence of propene in the feed. (c, h) Corresponding mass spectrometry data (m/z = 2, $H_2$; 28, CO; 30, NO; 32, $O_2$; 44, $CO_2$; 46, $C_3H_6$).

View Article Online
DOI: 10.1039/D0CP01064B

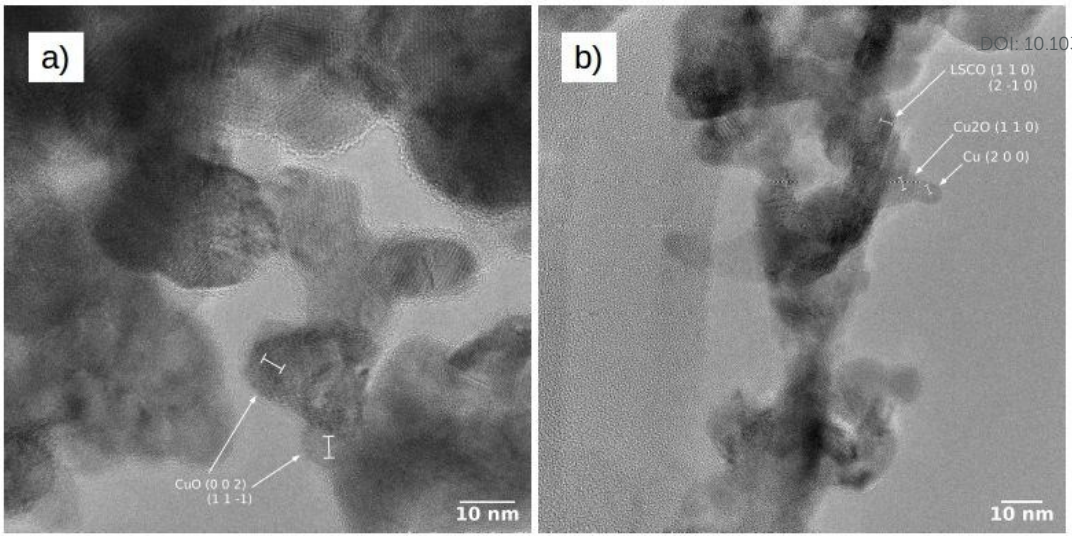


**Figure 1**

Journal Name ARTICLE

View Article Online
DOI: 10.1039/D0CP01064B

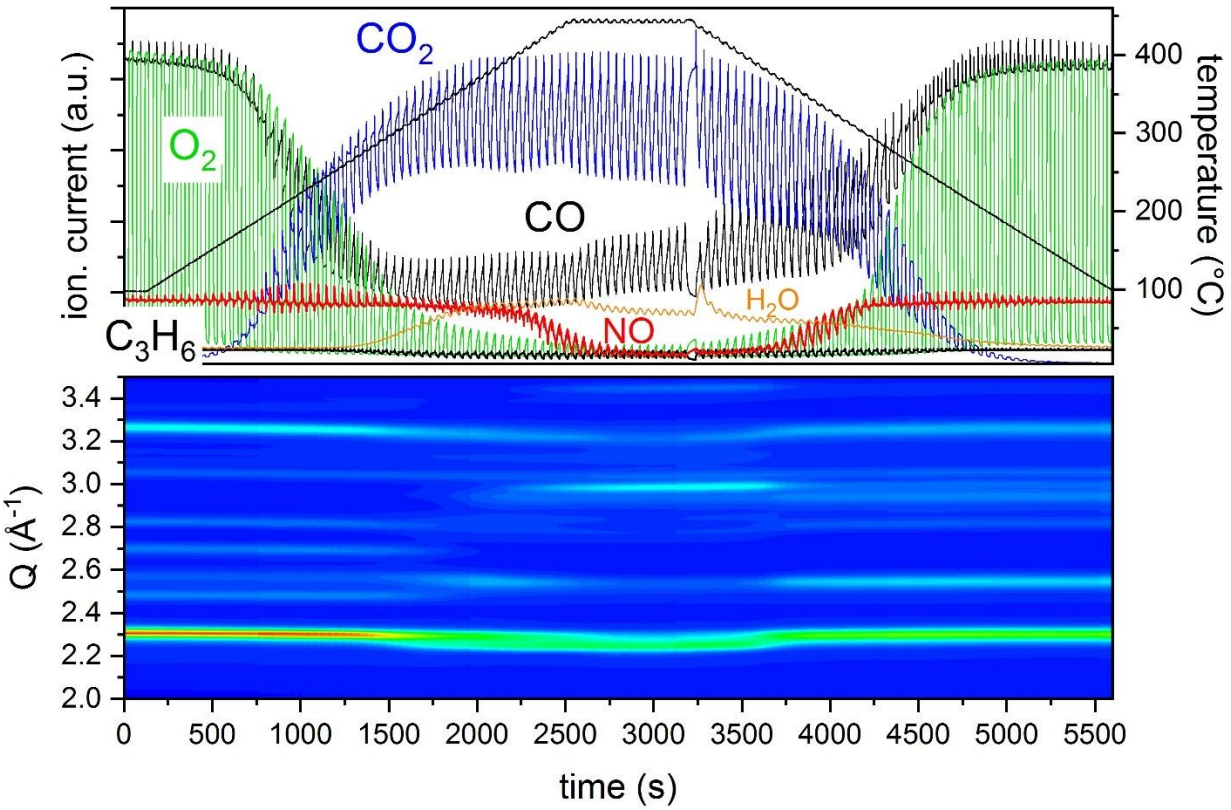


Figure 2

View Article Online
DOI: 10.1039/D0CP01064B

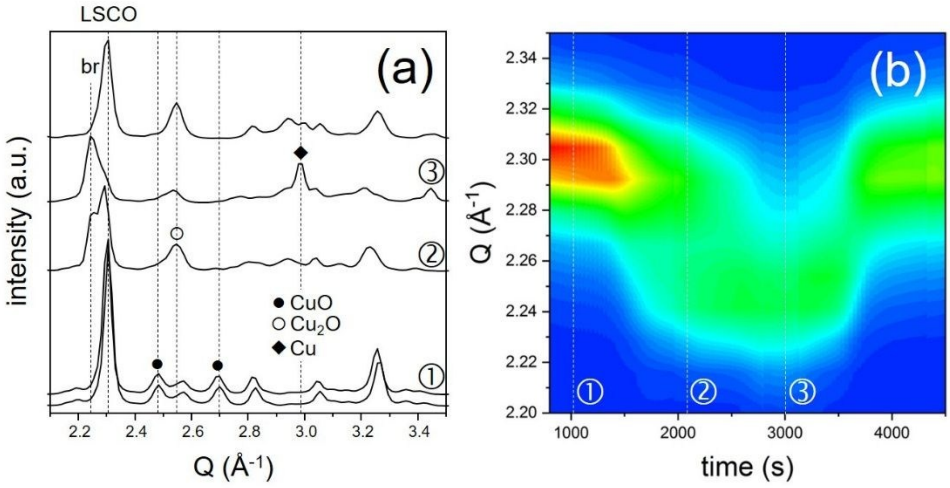


Figure 3

Journal Name ARTICLE

View Article Online
DOI: 10.1039/D0CP01064B

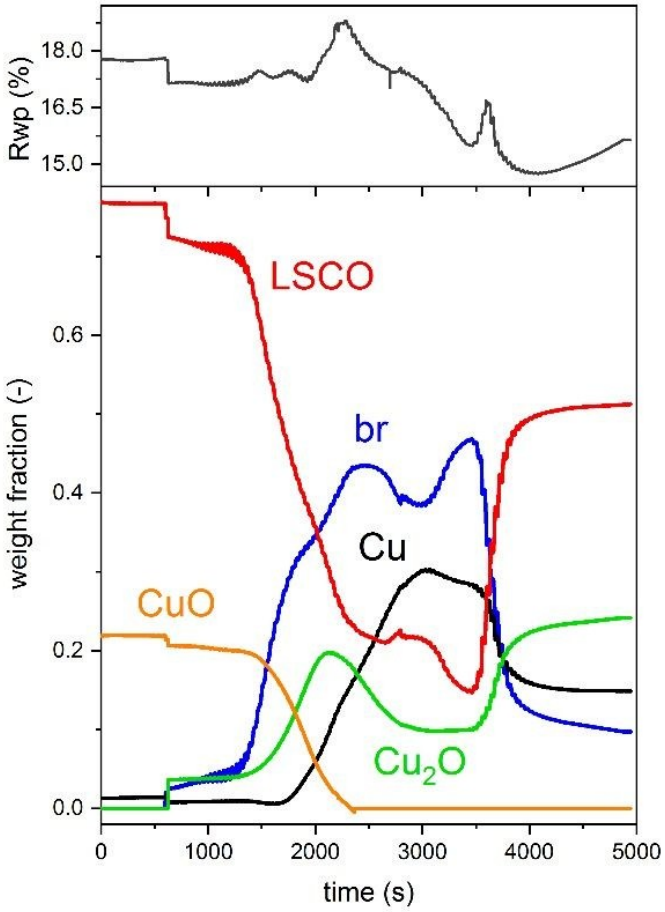


Figure 4

View Article Online
DOI: 10.1039/D0CP01064B



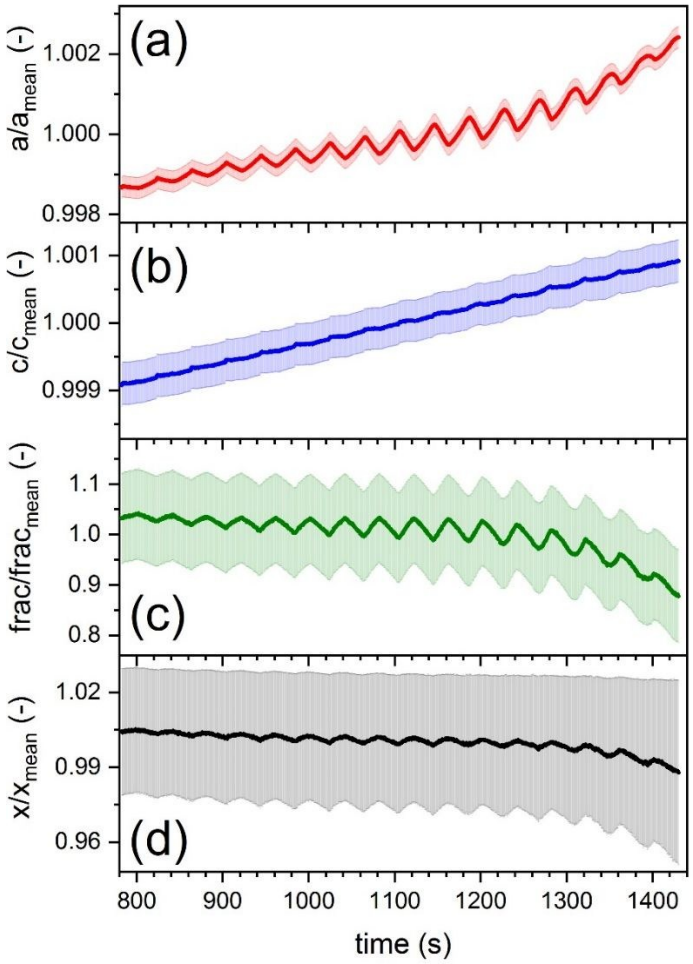


Figure 5

View Article Online
DOI: 10.1039/D0CP01064B

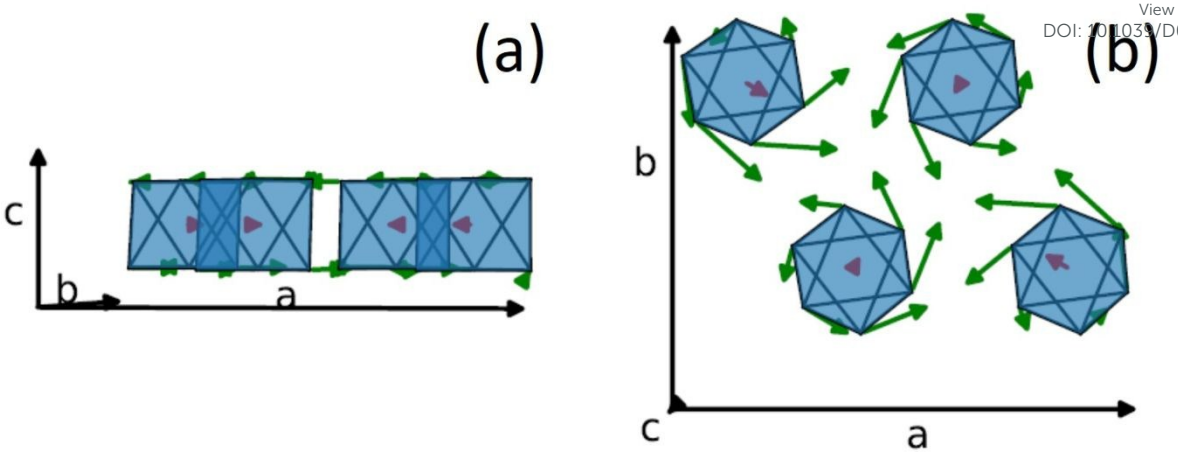


Figure 6

View Article Online
DOI: 10.1039/D0CP01064B



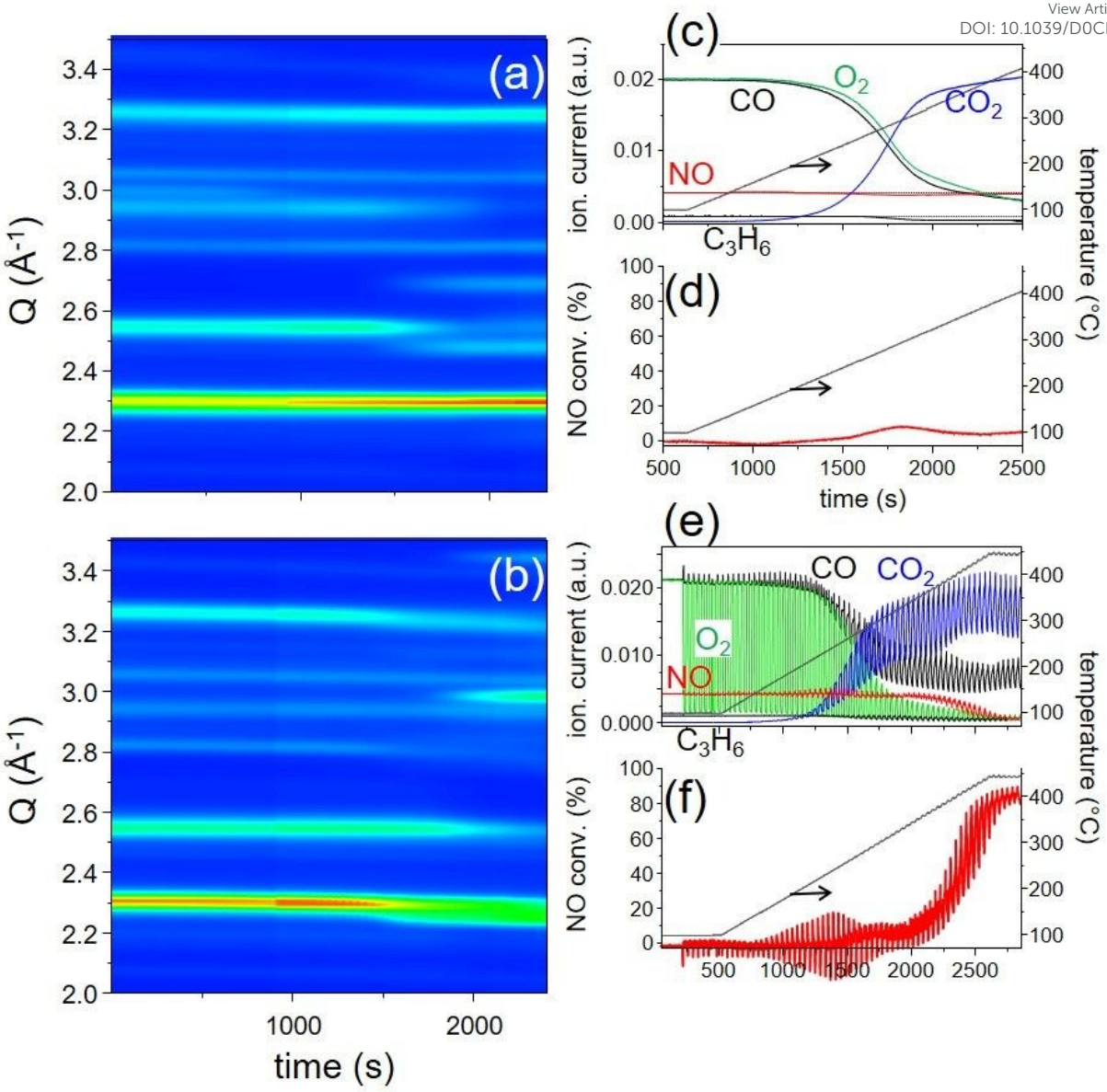


Figure 7

View Article Online
DOI: 10.1039/D0CP01064B



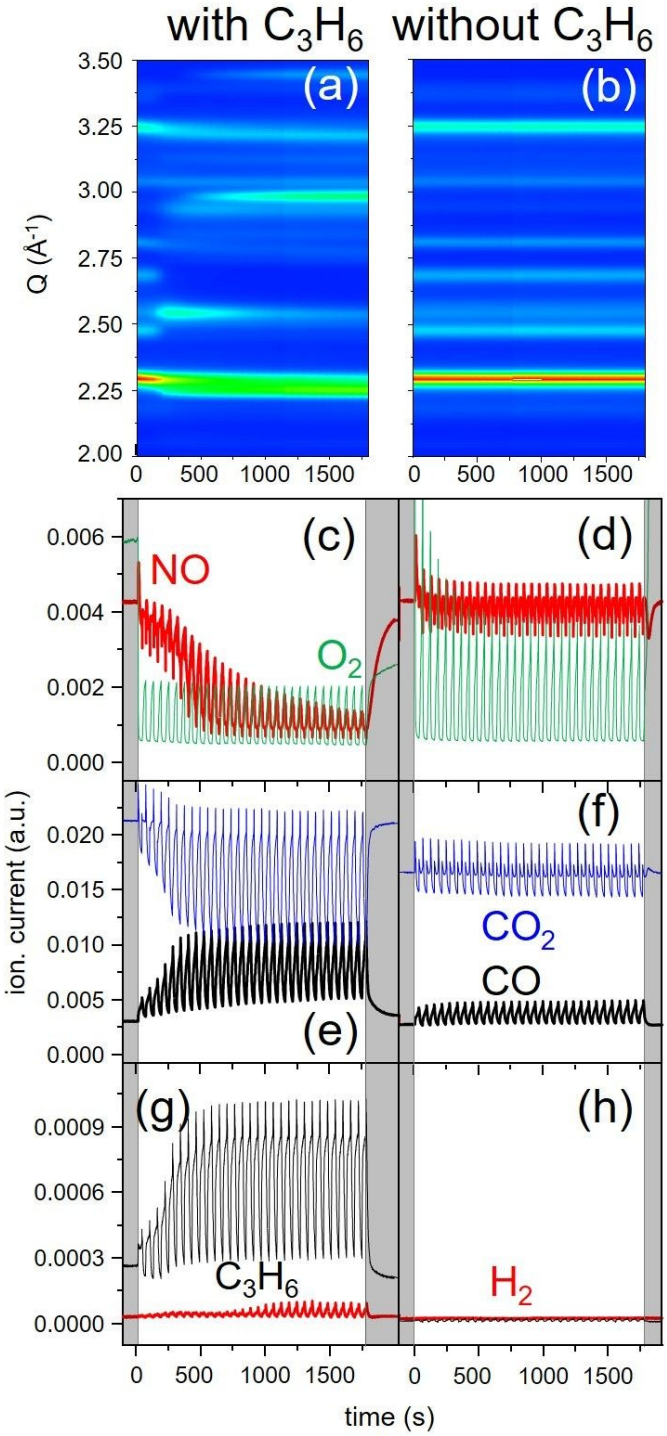


Figure 8